On the scattering of baroclinic Rossby waves by a ridge in a continuously stratified ocean

By G. W. OWEN[1]†, I. D. ABRAHAMS[2], A. J. WILLMOTT[1]
AND C. W. HUGHES[3]

[1]Department of Mathematics, Keele University, Staffordshire ST5 5BG, UK
[2]Department of Mathematics, University of Manchester, Manchester M13 9PL, UK
[3]Proudman Oceanographic Laboratory, Merseyside CH43 7RA, UK

In global ocean dynamics Rossby waves play a vital rôle in the long-term distribution of vorticity; knowledge of the interaction between these waves and topography is crucial to a full understanding of this process, and hence to the transportation of energy, mixing and ocean circulation. The interaction of baroclinic Rossby waves with abrupt topography is the focus of this study. In this paper we model the ocean as a continuously stratified fluid for which the linear theory predicts a qualitatively different structure for the wave modes than that predicted by barotropic or simple layered models, even if most of the density variation is confined to the thermocline. We consider the scattering of a westward-propagating baroclinic Rossby wave by a narrow ridge on the ocean floor, modelled by a line barrier of infinite extent, orientated at an arbitrary angle to the incident wave. Transmission and reflection coefficients for the propagating modes are found using both an algebraic method and, in the case where this breaks down, matched asymptotic expansions. The results are compared with recent analyses of satellite altimetry data.

1. Introduction

With the advent of satellite altimetry data leading to the routine production of global maps of the sea-surface topography, it has become possible to extract the signature of baroclinic Rossby waves in the sea-surface elevation (Chelton & Schlax 1996). By signature we refer to a field showing the orientation and rate of propagation of the crests and troughs of the travelling wave field. Thus, the wavelength and phase velocity of baroclinic Rossby waves can be derived in the world oceans, and this has led to renewed interest in the questions of the generation and propagation of such waves. Prior to altimetrically derived wave fields, observations of baroclinic Rossby waves were indirectly obtained from the analysis of long time series of the vertical displacement of isotherms at particular moorings within the thermocline (Emery & Magaard 1976). Time series data of this type were extremely sparse and therefore a global view of the propagation characteristics of baroclinic Rossby waves remained elusive.

TOPEX/POSEIDON altimeter data have revealed extratropical Rossby wave phase speeds greater than the linear long wave phase speed, by as much as a factor of two (Chelton & Schlax 1996) and eastward-propagating waves within the Antarctic Circumpolar Current (Hughes 1995). A similar picture regarding wave propagation

† Author to whom correspondence should be addressed: maa05@maths.keele.ac.uk

also emerges from the analysis of sea-surface temperature gradient data derived from the Along Track Scanning Radiometer in studies by Hughes, Jones & Carnochan (1998) and Hill, Robinson & Cipollini (2000). In this paper we are not concerned with the mechanisms that could explain the higher than expected phase speeds of westward-propagating extratropical baroclinic Rossby waves. Readers interested in this topic are directed to the studies by Killworth, Chelton & de Szoeke (1997), Killworth & Blundell (1999), Dewar (1998), Dewar & Morris (2000), and Qiu, Miao & Muller (1997). Instead, we are concerned with the influence of a submerged oceanic ridge on baroclinic Rossby wave propagation. Returning to the altimeter studies for guidance in this area, Hill *et al.* (2000) report that in the neighbourhood of major oceanic ridges (e.g. the mid-Atlantic ridge) the phase speed of the waves alters and that a phase discontinuity is exhibited in the wave pattern. Chelton & Schlax (1996) also note that ridge systems have an impact on the wave field; the amplitude of the first-mode baroclinic wave to the west of the ridge is considerably greater than that on the eastern side of the ridge.

To date, most of the theoretical studies addressing the effect of a ridge on Rossby waves consider a homogeneous or two-layer fluid in the presence of small-amplitude topography. For example, in Rhines (1969) the transmission and reflection of Rossby waves in a homogeneous fluid by abrupt topography is studied and it is demonstrated that small-amplitude topography can reflect the majority of incident wave energy in the low-frequency limit. Such a prediction, as will be shown, is not valid for a stratified fluid, and therefore results for homogeneous or piecewise-constant density profiles are of limited physical relevance to Rossby wave scattering. In further work on piecewise-constant density profiles the reflection and transmission of barotropic Rossby waves over a meridional top-hat ridge is addressed by Wang & Koblinsky (1994) and Huthnance (1981), and within the framework of basin modes, by Anderson & Killworth (1977). Wang & Koblinsky (1994) also study the energy conversion between the barotropic and baroclinic mode in a two-layer fluid when a wave is incident on the ridge. More generally, Rossby wave scattering by an infinitely long ridge of infinitesimal width rising vertically above the ocean floor (hereafter referred to as a 'vertical line barrier') has been studied, for a homogeneous fluid, by Mysak & LeBlond (1972) and Murphy & Willmott (1991). In Mysak & LeBlond (1972) the scatterer is a vertical line barrier of semi-infinite length spanning the entire fluid depth. Murphy & Willmott (1991) consider scattering by a meridional line barrier situated in an infinitely long zonal channel. In both these studies, the barrier is viewed as a prototypical representation of South America.

The scattering of topographic Rossby waves has been addressed in a continuously stratified fluid context by Schmidt & Johnson (1997). These authors study the scattering of topographic Rossby waves in a non-uniform continuously stratified ocean, where the scatterer is associated with: (i) an abrupt change in the cross-section of a sea-floor ridge; (ii) waves incident upon a ridge abutting a coast. In both of these problems the geometries support the possibility of incident wave energy being reflected back along the ridge, a fact that must be taken into account when calculating the scattered wave fields. Thus, Schmidt & Johnson (1997) are forced to generalize the isobath tracing method of Johnson (1989, 1991) to accommodate this type of geometry. In contrast with Schmidt & Johnson (1997) here we consider the scattering of baroclinic Rossby waves in an ocean of uniform depth for which the isobath tracing method is not applicable.

Pedlosky & Spall (1999) argue that steep topography is well represented by a submerged vertical line barrier. In reality, oceanic ridges have numerous gaps and in

a series of papers (Pedlosky & Spall 1999; Pedlosky 2000*a*, *b*, 2001) Pedlosky considers the transmission and reflection of Rossby waves across a submerged meridional line barrier (and, indeed, a barrier of non-zero finite width) with gaps. All these papers adopt quasi-geostrophic theory in either a homogeneous or two-layer fluid, and the key point that emerges is that the nature of the transmission depends strongly on the nature of the gaps in the barrier. The waves propagate through the barrier without change of vertical structure when the gaps extend throughout the depth of the fluid. However, when the gaps in the barrier are partial and extend only over a single layer there is significant transformation of the vertical structure of the wave as it traverses the barrier.

In this paper we consider the scattering of an incident baroclinic Rossby wave by a submerged line barrier of arbitrary orientation and of infinite length in a continuously stratified fluid. The inclusion of continuous stratification is intended to offer a substantial improvement in the modelling over previous studies. However, it will result in an infinite number of modes in the modal structure, which presents an appreciable additional difficulty in obtaining a solution by algebraic means. A model of this type will, of course, support energy conversion between modes, the precise structure of which is to be determined. For mathematical convenience, and ease of exposition, henceforth we assume linear stratification (i.e. constant N_0) although the methods employed in this article are applicable to arbitrary stratification. No qualitative differences in the scattered wave field are expected in more physically realistic cases. Certainly, typical density profiles in the ocean usually have rapid variation only in a region near the free surface (i.e. within the thermocline), whereas topographic variations tend to be confined relatively near to the ocean floor where the buoyancy (Brunt–Väisälä) frequency is essentially constant. We believe that a constant buoyancy frequency is therefore a reasonable first approximation to realistic stratification, at least for small-amplitude topography. Nevertheless it would be prudent to confirm these ideas elsewhere.

Two distinct methods are presented for solving the present boundary value problem. First, a modal matching technique is described, which is a method frequently adopted by the research community working on linear water wave scattering by barriers (see, for example, McIver 1985; Porter & Evans 1995). Unfortunately, the method converges slowly, and becomes impracticable, in the limits of an infinitesimal-height barrier or a near surface-piercing barrier. In the former case, we also present a matched asymptotic solution technique, based on a procedure now routine in acoustic and elastic wave scattering problems (see e.g. Abrahams & Wickham 1992).

The plan of the paper is as follows. In §2 the scattering problem is formulated. Section 3 describes the mode-matching solution technique and highlights its short-comings. A matched asymptotic Green's function solution is derived in §4 for the case of scattering by an infinitesimal-height barrier. In §5 numerical results are presented using the two approaches of §§3 and 4, showing the reflection and transmission coefficients of the dominant vertical modes for a variety of barrier orientations and heights. Finally, §6 contains suggestions for future research and a summary of the results.

2. Formulation of the problem

2.1. *Overview and equation of motion*

Rossby waves, or planetary waves, play a crucial rôle in unsteady global oceanic circulation. These waves propagate in regions of non-uniform ambient potential
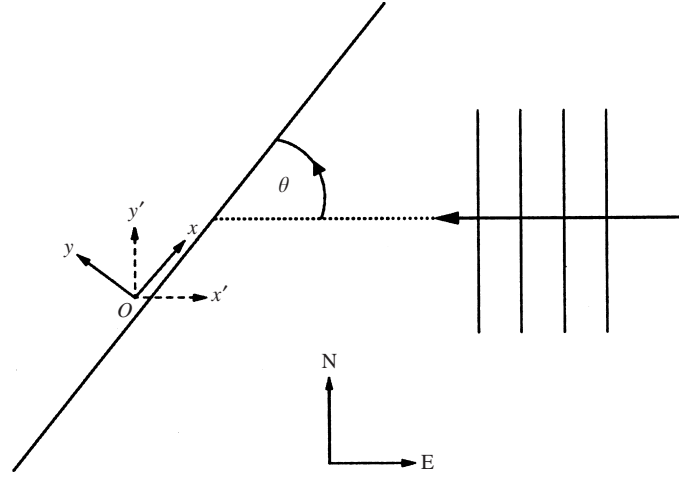
FIGURE 1. Geometry of barrier and incident wave.

vorticity by conserving their potential vorticity as they do so. Bottom topography and the variation of the Coriolis parameter (a quantity proportional to the normal component of the Earth's angular velocity at the surface, see, for example, Cushman-Roisin 1994) with latitude both give rise to a non-uniform ambient potential vorticity field. Baroclinic Rossby waves typically propagate at low speeds (relative to barotropic Rossby waves, inertial Poincaré waves or coastally trapped Kelvin waves) and have periods of the order of six months or longer. Further details may be found in Pedlosky (1979). We are interested in the interactions of these waves with the topography of the ocean floor, in particular ridges.

As our initial model we consider the ocean to be a continuously stratified Boussinesq fluid occupying $-H \leqslant z \leqslant 0$, on a mid-latitude β-plane, with a linearized dependence of Coriolis parameter on the meridional coordinate, y', i.e. $f_0 + \beta y'$, where f_0 and β are constants and a right-handed coordinate frame $Ox'y'z$ has been introduced, with Ox' directed eastward and Oy' northward. For convenience, we shall introduce a rotated coordinate system $Oxyz$ as shown in figure 1. Then the ocean ridge is modelled by an infinitely thin bottom-standing barrier occupying the plane $y = 0$ and a fraction of the total depth of the ocean, $-H \leqslant z < -\mu H, 0 < \mu < 1$, whose orientation makes an angle θ with the x'-axis. Thus a meridional ridge corresponds to an angle of $\theta = 90°$. A westward-propagating long baroclinic Rossby wave of vertical mode 1 is incident on the barrier. We wish to find the scattered field. We shall also assume the flow is quasi-geostrophic, i.e. the horizontal components of the velocity field in the x'- and y'-directions respectively are given by

$$u = -\frac{1}{\rho_0 f_0} \frac{\partial p'}{\partial y'} \quad \text{and} \quad v = \frac{1}{\rho_0 f_0} \frac{\partial p'}{\partial x'}, \tag{2.1}$$

where $p'(x', y', z, t)$ is the pressure in the fluid and $\rho_0(z)$ is the density in the undisturbed fluid. For this, strictly speaking, we require the topography to be of infinitesimal amplitude, i.e. $1 - \mu \ll 1$, a point discussed in Pedlosky (1979). The pressure field then satisfies the linearized Rossby wave equation:

$$\frac{\partial}{\partial t} \left\{ \nabla_H^2 p' + f_0^2 \frac{\partial}{\partial z} \left[\frac{1}{N_0^2} \frac{\partial p'}{\partial z} \right] \right\} + \beta \frac{\partial p'}{\partial x'} = 0, \tag{2.2}$$

where $N_0(z)$ is the Brunt–Väisälä frequency and ∇_H^2 is the two-dimensional horizontal Laplacian. A full derivation of the linearized Rossby wave equation may again be found in Pedlosky (1979, chap. 3). We shall seek time-harmonic wave solutions with periods of several months or longer, and therefore write

$$p'(x', y', z, t) = \text{Re}\left\{p(x, y, z) \exp(-i\omega t)\right\}, \tag{2.3}$$

where x and y are aligned in the direction parallel to, and normal to, the barrier, respectively and $\omega > 0$ is the constant angular frequency.

2.2. *Modal decomposition*

We shall seek modal solutions of the form

$$p(x, y, z) = \exp(ikx + ily)\Gamma(z), \tag{2.4}$$

where k and l are constant wavenumbers. Applying the method of separation of variables (in the horizontal and vertical directions) in (2.2) we obtain the Sturm–Liouville eigenvalue problem for Γ, namely

$$f_0^2 \frac{d}{dz}\left(\frac{1}{N_0^2}\frac{d}{dz}\Gamma(z)\right) + \lambda^2\Gamma(z) = 0, \quad \Gamma'(0) = \Gamma'(-H) = 0, \tag{2.5}$$

with λ^2 the separation constant. The boundary conditions in (2.5) express the conditions of the vanishing of the vertical velocity component on the sea floor and the undisturbed sea surface (commonly referred to as the 'rigid lid' boundary condition). For constant N_0 the eigenvalue problem may be solved analytically and the orthonormal vertical modes, $\Gamma_n(z)$, are given by

$$\Gamma_n(z) = \left(\frac{\epsilon_n}{H}\right)^{1/2}\cos\frac{n\pi z}{H} \tag{2.6}$$

with $\epsilon_0 = 1$, $\epsilon_n = 2$, $n = 1, 2, 3, \ldots$. The associated eigenvalues, λ_n, are

$$\lambda_n = \frac{n\pi f_0}{HN_0} = \frac{\pi}{r_n} = \frac{f_0}{(gh_n)^{1/2}}, \tag{2.7}$$

where the r_n are the internal Rossby radii of deformation and the h_n are the effective (equivalent) depths. Substituting these separation constants and the ansatz given in (2.4) into (2.2) we find that the wavenumbers k_n and l_n for each mode satisfy the dispersion relation

$$\frac{\omega}{\beta} = \frac{l_n\sin\theta - k_n\cos\theta}{k_n^2 + l_n^2 + f_0^2/gh_n}. \tag{2.8}$$

From the symmetry of the geometry of the problem it is clear that the spatially harmonic variation of the pressure in the x-direction (along the ridge) is fixed by the spatial variation of the incident Rossby wave in that direction (i.e. the x wavenumber must be constant). Thus the k_n must be the same for all n and the dispersion relation (2.8) may be considered to be a quadratic equation for the wavenumbers l_n. It is well known (see, for example, Pedlosky 1979) that two distinct real roots of the dispersion relation represent long and short Rossby waves which have westward phase velocity but westward and eastward group velocities respectively. We shall denote the wavenumber which decays or has outward-going group velocity in the region $y > 0$ by l_n and that which decays or has outward group velocity in the region $y < 0$ by s_n. We shall write the pressure field associated with the incident baroclinic (mode 1) Rossby wave as $\exp(ik_1 x + il_1 y)\,\Gamma_1(z)$, where $k_1 = k\cos\theta$, $l_1 = -k\sin\theta$ and k is the

wavenumber of a westward-propagating long baroclinic Rossby wave of frequency ω. Thus, we may write the total pressure field as the sum of the scattered field and the incident Rossby wave as

$$p(x,y,z) = \begin{cases} \exp(ik_1 x + il_1 y)\Gamma_1(z) + \displaystyle\sum_0^\infty a_n \exp(ik_1 x + is_n y)\Gamma_n(z), & y < 0, \\[2ex] \displaystyle\sum_0^\infty b_n \exp(ik_1 x + il_n y)\Gamma_n(z), & y > 0, \end{cases} \tag{2.9}$$

where $\{a_n\}$ and $\{b_n\}$ are the reflection and transmission coefficients, respectively, to be determined.

2.3. *Boundary conditions*

Above the barrier, in the region $-\infty < x < \infty$, $y = 0$, $-\mu H < z < 0$ we shall impose continuity of both x and y components of the velocity field. From (2.1) these matching conditions are, in fact, equivalent to continuity of pressure and the velocity component parallel to the barrier. We shall also assume that the barrier, which occupies $-\infty < x < \infty$, $y = 0$, $-H < z < -\mu H$, is impermeable and thus that there is no normal flow through it. We may now, using the quasi-geostrophic approximation given in (2.1), express these boundary conditions in terms of the coefficients a_n and b_n given in (2.9). From the continuity conditions we have, for $-\mu H < z < 0$,

$$\sum a_n \Gamma_n(z) + \Gamma_1(z) = \sum b_n \Gamma_n(z), \tag{2.10}$$

$$\sum a_n s_n \Gamma_n(z) + l_1 \Gamma_1(z) = \sum b_n l_n \Gamma_n(z), \tag{2.11}$$

where for notational convenience, we have suppressed the range of the summation index, which goes from $n = 0$ to $n = \infty$ unless otherwise stated. Similarly, the impermeability condition gives us, for $-H < z < -\mu H$,

$$\sum a_n \Gamma_n(z) + \Gamma_1(z) = 0, \tag{2.12}$$

$$\sum b_n \Gamma_n(z) = 0. \tag{2.13}$$

From (2.10), (2.12) and (2.13) it may be seen that the equation

$$\sum a_n \Gamma_n(z) + \Gamma_1(z) = \sum b_n \Gamma_n(z) \tag{2.14}$$

holds throughout the entire depth of the ocean, $-H < z < 0$.

3. Algebraic method of solution

3.1. *Algebraic form of the boundary conditions*

In order to find the transmission and reflection coefficients of the scattered modes it is now necessary to determine the coefficients a_n and b_n. Multiplying (2.14) by $\Gamma_m(z)$, integrating over $-H < z < 0$ and using the orthonormality of the eigenfunctions, $\Gamma_j(z)$, we obtain

$$a_n + \delta_{n1} = b_n, \quad n = 0, 1, 2, \ldots, \tag{3.1}$$

where δ_{ij} is the Kronecker delta. This reflects the symmetry in the geometry, but due to the anisotropy in the equation of motion, *does not* provide information about

the partitioning of energy into the modes. Upon multiplying (2.12) by $\Gamma_m(z)$ and integrating over the range $-H < z < -\mu H$ we obtain

$$(\boldsymbol{I} - \boldsymbol{C})\boldsymbol{a} + (\boldsymbol{I} - \boldsymbol{C})\boldsymbol{e}_2 = \boldsymbol{0}, \tag{3.2}$$

where $\boldsymbol{a}$ denotes a column vector $\{a_n\}$, $\boldsymbol{e}_n$ denotes the column vector with zero elements except for a 1 in the nth row, $\boldsymbol{I}$ is the identity matrix and the infinite symmetric matrix $\boldsymbol{C}$ is defined by

$$C_{ij} = \int_{-\mu H}^{0} \Gamma_i(z)\Gamma_j(z)\mathrm{d}z = C_{ji}. \tag{3.3}$$

Similarly, integrating (2.11) and eliminating the b_n using (3.1) we obtain

$$\boldsymbol{C}(\boldsymbol{L} - \boldsymbol{S})\boldsymbol{a} = \boldsymbol{0}, \tag{3.4}$$

where the infinite diagonal matrices $\boldsymbol{L}$ and $\boldsymbol{S}$ have the wavenumbers l_n and s_n as their diagonal entries. It may be seen then, from (3.2) and (3.4), that if either of the operators $\boldsymbol{C}$ and $\boldsymbol{I} - \boldsymbol{C}$ is invertible then the problem does not have a solution. It is, however, easy to show that this is not the case. Denoting the restriction of $\Gamma_n(z)$ to $(-\mu H, 0)$ by $\gamma_n(z)$, i.e.

$$\gamma_n(z) = \begin{cases} \Gamma_n(z), & z \in [-\mu H, 0] \\ 0, & z \in [-H, -\mu H), \end{cases} \tag{3.5}$$

and again using the orthonormality of the vertical eigenfunctions we may express $\gamma_i(z)$ as a generalized Fourier series

$$\gamma_i(z) = \sum_j \left[\int_{-H}^{0} \gamma_i(s)\Gamma_j(s)\mathrm{d}s \right] \Gamma_j(z) = \sum_j C_{ij}\Gamma_j(z). \tag{3.6}$$

Thus we have

$$
\begin{aligned}
C_{ij} &= \int_{-\mu H}^{0} \gamma_i(s)\Gamma_j(s)\mathrm{d}s \\
&= \int_{-\mu H}^{0} \left[\sum_k C_{ik}\Gamma_k(s) \right] \Gamma_j(s)\mathrm{d}s \\
&= \sum_k C_{ik} \left[\int_{-\mu H}^{0} \Gamma_k(s)\Gamma_j(s)\mathrm{d}s \right] = \sum_k C_{ik}C_{kj}, \tag{3.7}
\end{aligned}
$$

and hence $\boldsymbol{C}^2 = \boldsymbol{C}$. Therefore, except in the trivial cases where $\mu = 0$ and $\mu = 1$, when $\boldsymbol{C} = \boldsymbol{0}$ and $\boldsymbol{C} = \boldsymbol{I}$ respectively, we find that 1 and 0 are the only eigenvalues of $\boldsymbol{C}$. Equations (3.2) and (3.4) may be rewritten as

$$\boldsymbol{a} + \boldsymbol{e}_2 \in \ker(\boldsymbol{I} - \boldsymbol{C}) \quad \text{and} \quad (\boldsymbol{L} - \boldsymbol{S})\boldsymbol{a} \in \ker \boldsymbol{C}, \tag{3.8}$$

where $\ker \boldsymbol{C}$ denotes the kernel of $\boldsymbol{C}$. We shall solve these equations by approximately constructing the kernels by consideration of the eigenvalues and eigenvectors of the truncated system.

3.2. *Solution of the truncated system*

Equations (3.2) and (3.4) may be considered to form two infinite systems of algebraic equations. Suppose we truncate these equations to form two systems of, say, M
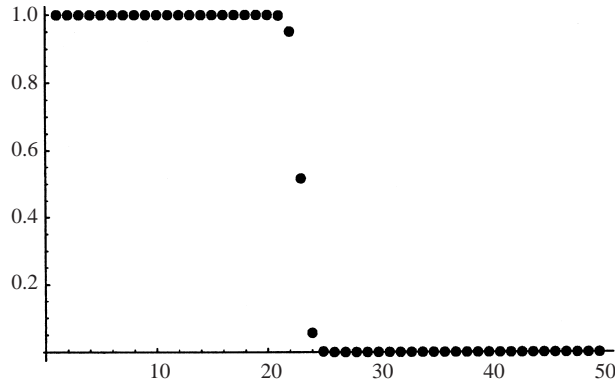
FIGURE 2. Eigenvalues of $\widetilde{\mathbf{C}}$ with $M = 50$ and $\mu = 0.45$.

equations. We shall denote the truncation of $\mathbf{C}$ to a real symmetric square matrix of size $M \times M$ by $\widetilde{\mathbf{C}}$, and the similarly truncated vectors $\boldsymbol{a}$ and $\boldsymbol{e}_2$ by $\tilde{\boldsymbol{a}}$ and $\tilde{\boldsymbol{e}}_2$. It is now possible to calculate the M eigenvalues, v_n and eigenvectors $\boldsymbol{v}_n$, $n = 1, 2, \ldots, M$ of $\widetilde{\mathbf{C}}$. The eigenvalues of such a matrix, with $M = 50$, are shown in figure 2. This is a quite typical distribution of eigenvalues, with all except a small number of eigenvalues being either close to 1 or close to 0. We also suppose, without loss of generality, that $v_n \leqslant v_{n-1}$ and that m is such that $v_m \geqslant 0.5$ and $v_{m+1} < 0.5$. We may then partition the eigenvectors into the sets

$$J = \{\boldsymbol{v}_n : 1 \leqslant n \leqslant m\} \quad \text{and} \quad K = \{\boldsymbol{v}_n : m < n \leqslant M\}. \tag{3.9}$$

It is found by numerical experiment that the ratio of the number of elements in J to M (where M is the number of elements in $J \cup K$) is close to μ. This result is extremely plausible but hard to prove. Clearly, when $\mu = 1$ then $\mathbf{C} = \boldsymbol{I}$ and all the eigenvalues are 1, and when $\mu = 0$ then $\mathbf{C} = \mathbf{0}$ and all the eigenvalues are 0.

The span of K is a finite-dimensional approximation to the kernel of $\mathbf{C}$ in the sense that for any set of coefficients, α_n, such that

$$\boldsymbol{v} = \sum_{n=1}^{M} \alpha_n \boldsymbol{e}_n \in \text{span } K \tag{3.10}$$

we have, above the barrier,

$$\sum_{n=1}^{M} \alpha_n \Gamma_{n-1}(z) \simeq 0, \quad z \in (-\mu H, 0). \tag{3.11}$$

Although it is possible to construct a vector in the span of K for which the above approximate equation does not hold ($\boldsymbol{v} = \boldsymbol{v}_m$ is the obvious example), extensive numerical experiments have shown typically that such special cases do not arise. Alternatively, the span of J is an approximation to the kernel of $\boldsymbol{I} - \mathbf{C}$ in the sense that for a typical vector $\boldsymbol{v} \in \text{span } J$, given by

$$\boldsymbol{v} = \sum_{n=1}^{M} \beta_n \boldsymbol{e}_n, \tag{3.12}$$

say, we have

$$\sum_{n=1}^{M} \beta_n \Gamma_{n-1}(z) \simeq 0 \quad \text{for} \quad z \in (-H, -\mu H). \tag{3.13}$$

Thus, if we wish to solve approximately (3.4) we may write

$$\boldsymbol{a} = (\boldsymbol{S} - \boldsymbol{L})^{-1} \sum_{n=m+1}^{M} \alpha_n \boldsymbol{v}_n \tag{3.14}$$

where the coefficients α_m are to be determined. Substituting this form into the impermeability condition in (3.2) we find

$$(\widetilde{\boldsymbol{C}} - \boldsymbol{I}) \sum_{n=m+1}^{M} \alpha_n (\boldsymbol{S} - \boldsymbol{L})^{-1} \boldsymbol{v}_n = (\boldsymbol{I} - \widetilde{\boldsymbol{C}}) \boldsymbol{e}_2. \tag{3.15}$$

From the symmetry of $\boldsymbol{C}$ we may diagonalize the matrix $\boldsymbol{I} - \widetilde{\boldsymbol{C}}$ and write it in the form

$$\boldsymbol{I} - \widetilde{\boldsymbol{C}} = \boldsymbol{U}\boldsymbol{D}\boldsymbol{U}^T, \tag{3.16}$$

where the matrix $\boldsymbol{U}$ is orthogonal and the diagonal matrix $\boldsymbol{D}$ is defined by

$$D_{ij} = \begin{cases} 1 - v_i, & i = j, \\ 0, & i \neq j. \end{cases} \tag{3.17}$$

Upon pre-multiplication by $\boldsymbol{U}^{-1}$ (3.15) becomes

$$\boldsymbol{D}\boldsymbol{U}^T (\boldsymbol{L} - \boldsymbol{S})^{-1} \sum_{n=m+1}^{M} \alpha_n \boldsymbol{v}_n = \boldsymbol{D}\boldsymbol{U}^T \boldsymbol{e}_2. \tag{3.18}$$

It may be seen that whenever the eigenvalue $v_i \simeq 1$ the matrix element D_{ii} is negligible and the constraint imposed by the ith row of the vector equation can be considered to be trivially satisfied for all α_n. Thus, if we neglect the first m rows of (3.18) we are left with a system of $M - m$ equations for the $M - m$ unknowns, $\alpha_{m+1}, \ldots, \alpha_M$, which may be solved.

Truncation errors in this approximate solution arise either from a neglected term of the form $1 - v_i$ in $\boldsymbol{D}$ being non-zero or the form of $\boldsymbol{a}$ given in (3.14) not satisfying (3.4) exactly. In each case the size of the error is dependent upon the size of the coefficients of those eigenvectors with eigenvalues away from 1 or 0. These eigenvectors have no physical relevance to the problem, being a result only of the truncation process, and in practice the relevant coefficients, and the associated errors, tend to zero with increasing truncation number.

4. Asymptotic solution

4.1. *Modified equation of motion and scalings*

As previously discussed, the algebraic method of solution outlined above fails in the case where the barrier occupies either a very large or very small proportion of the total depth of the fluid. In these cases the partition of the eigenvectors into the sets J and K is uneven. When the barrier is small $(1 - \mu \ll 1)$ the ratio of 'large' eigenvalues to 'small' eigenvalues is large, J is much larger than K and the convergence is very slow due the paucity of elements in K. However, the latter case can effectively be dealt with by employing the method of matched asymptotic expansions.

We shall assume that the pressure field is time harmonic, and has its spatial variation in the longshore direction, x, fixed from the incident wave. Furthermore, in order to simplify the equation of motion we introduce the carrier-wave transformation to remove the β-effect anisotropy from (2.2). Thus we write

$$p'(x', y', z, t) = \text{Re}\{\tilde{p}(y, z) \exp(\mathrm{i}k_1 x + \mathrm{i}\gamma y + \mathrm{i}\omega t)\} \quad \text{with} \quad \gamma = -\frac{\beta \sin \theta}{2\omega} \tag{4.1}$$

and (2.2) becomes

$$\frac{\partial^2 \tilde{p}}{\partial y^2} + \frac{f_0^2}{N_0^2} \frac{\partial^2 \tilde{p}}{\partial z^2} + K^2 \tilde{p} = 0 \tag{4.2}$$

where the wavenumber K is given by

$$K^2 = \left\{ \frac{\beta^2 \sin^2 \theta}{4\omega^2} + \frac{\beta k_1 \cos \theta}{\omega} - k_1^2 \right\}. \tag{4.3}$$

It may be shown that if the physical parameters in (4.3) are chosen such that the ocean basin supports propagating Rossby waves whose wavenumber in the direction of the ridge is k_1, we have $K^2 > 0$, and thus K is real.

In the inner region, where the dynamics of the flow are dominated by the topography, we scale the variables by the height of the ridge, $1 - \mu$, i.e.

$$Y = \frac{f_0 y}{(1 - \mu)HN_0} \quad \text{and} \quad Z = \frac{z + H}{(1 - \mu)H}. \tag{4.4}$$

The coefficients in (4.4) are chosen for convenience, i.e. to reduce the operator in (4.2) to the Laplacian. In the outer region the dominant length scale is the wavelength of the propagating Rossby waves and hence it is appropriate to employ the scalings

$$\bar{y} = Ky \quad \text{and} \quad \bar{z} = \frac{KN_0 z}{f_0}. \tag{4.5}$$

For convenience we also define the non-dimensional ocean depth, h, an additional non-dimensional vertical coordinate, η, and the polar coordinates $\bar{r}$, R and θ by

$$h = \frac{KN_0 H}{f_0}, \quad \eta = \bar{z} + h \quad \text{and} \quad \bar{r} \exp \mathrm{i}\theta = \epsilon R \exp \mathrm{i}\theta = \eta + \mathrm{i}\bar{y}, \tag{4.6}$$

respectively. Thus, defining the non-dimensional small parameter ϵ by

$$\epsilon = N_0 HK(1 - \mu)f_0^{-1}, \tag{4.7}$$

we have

$$\bar{y} = \epsilon Y \quad \text{and} \quad \eta = \epsilon Z. \tag{4.8}$$

We now use this small parameter in order to express the pressure field in the inner and outer regions as perturbation expansions. *A priori* knowledge about such physical problems suggests that this expansion should include not only terms like ϵ^n, $n \geqslant 0$, but also those of the form $\epsilon^n/(\log \epsilon + K)$, where K is some constant to be determined. This is discussed in some detail in Crighton *et al.* (1992, §6.8) but formal matching with both sets of gauge functions leads to much complexity in both notation and algebra. Henceforth, for ease of exposition we omit the second set of gauge functions, treat $\log \epsilon$ terms as constants, and just match in ϵ and its integer powers. This procedure is a good deal simpler to follow and has been shown to be equivalent to the full matching process (Abrahams 1987). Thus, scaling out the normalization factor of

$(2/H)^{1/2}$ for convenience we pose, in the inner region,

$$\left(\frac{H}{2}\right)^{1/2} p(y,z) = P^{(i)}(Y,Z) + P(Y,Z) = P^{(i)}(Y,Z) + \sum_{n=0}^{\infty} \epsilon^n P_n(Y,Z), \qquad (4.9)$$

in which the rescaled incident baroclinic Rossby wave term is

$$P^{(i)}(Y,Z) = -\exp\{-\mathrm{i}k\sin\theta(1-\mu)HN_0 Y f_0^{-1}\}\cos\{\pi(1-\mu)Z\}. \qquad (4.10)$$

Similarly, in the outer region we expect

$$\left(\frac{H}{2}\right)^{1/2} p(y,z) = \overline{p}(\overline{y},\overline{z}) = \overline{p}^{(i)}(\overline{y},\overline{z}) + \sum_{n=0}^{\infty} \epsilon^n \overline{p}_n(\overline{y},\overline{z}). \qquad (4.11)$$

4.2. Outer problem

Rewriting (4.2) in terms of the outer variables we obtain

$$\frac{\partial^2 \overline{p}}{\partial \overline{y}^2} + \frac{\partial^2 \overline{p}}{\partial \overline{z}^2} + \overline{p} = 0, \qquad (4.12)$$

and on these length scales the barrier will be vanishingly small. Thus, in the absence of the barrier we may first find a Green's function, $g(\overline{y}_0, \overline{z}_0; \overline{y}, \overline{z})$, which satisfies the equation

$$\frac{\partial^2 g}{\partial \overline{y}_0^2} + \frac{\partial^2 g}{\partial \overline{z}_0^2} + g = \delta(\overline{z}_0 - \overline{z})\delta(\overline{y}_0 - \overline{y}). \qquad (4.13)$$

We shall also impose the impermeable bottom and rigid lid boundary conditions on the Green's function solution, i.e. that

$$\frac{\partial g}{\partial \overline{z}_0}(\overline{y}_0, 0; \overline{z}, \overline{y}) = \frac{\partial g}{\partial \overline{z}_0}(\overline{y}_0, -h; \overline{z}, \overline{y}) = 0, \qquad (4.14)$$

and the same radiation conditions as the scattered wave field. Using the usual Fourier transform techniques it is straightforward to show that the Green's function may be written

$$g(\overline{y}_0, \overline{z}_0; \overline{y}, \overline{z}) = \frac{1}{2\pi} \int_{-\infty}^{\infty} \exp\{\mathrm{i}\alpha(\overline{y} - \overline{y}_0)\} G(\alpha, \overline{z}_0; \overline{z}) \mathrm{d}\alpha \qquad (4.15)$$

where G is given by

$$G(\alpha, \overline{z}_0; \overline{z}) = \begin{cases} -\dfrac{\cosh\left[\{\overline{z} + h\}\gamma(\alpha)\right]\cosh\left[\overline{z}_0\gamma(\alpha)\right]}{\gamma(\alpha)\sinh\left[h\gamma(\alpha)\right]}, & \overline{z}_0 > \overline{z}, \\[4mm] -\dfrac{\cosh\left[\{\overline{z}_0 + h\}\gamma(\alpha)\right]\cosh\left[\overline{z}\gamma(\alpha)\right]}{\gamma(\alpha)\sinh\left[h\gamma(\alpha)\right]}, & \overline{z}_0 < \overline{z}, \end{cases} \qquad (4.16)$$

with $\gamma(\alpha) = (\alpha^2 - 1)^{1/2}$.

We shall now apply Green's theorem to the region $\mathcal{V}$, the interior of the contour $\partial\mathcal{V}$ shown in figure 3, where the vertical sections of the contour are located a large distance from the barrier. Doing so, we obtain

$$\int_{\partial\mathcal{V}} \left\{ g\frac{\partial \overline{p}}{\partial n} - \overline{p}\frac{\partial g}{\partial n} \right\} \mathrm{d}L_0 = \int_{\mathcal{V}} \left\{ g\nabla^2 \overline{p} - \overline{p}\nabla^2 g \right\} \mathrm{d}S_0 = -\overline{p}(\overline{y},\overline{z}), \qquad (4.17)$$

where $\partial/\partial n$ denotes the outward normal derivative. From the boundary conditions
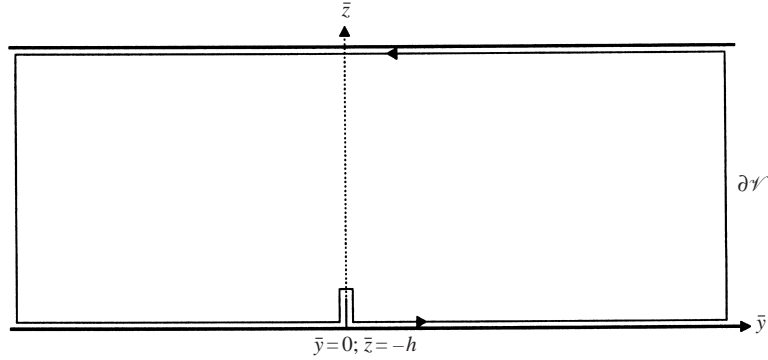
FIGURE 3. Contour used for the application of Green's theorem (4.17).

satisfied by $\bar{p}$ and g at the ocean surface and floor, and the outward radiation condition as $y \to \pm\infty$, we may rewrite the first integral in (4.17) as

$$\bar{p}(\bar{y}, \bar{z}) = \bar{p}^{(i)}(\bar{y}, \bar{z}) - \int_{-h}^{-\mu h} \left\{ \frac{\partial \bar{p}}{\partial \bar{y}_0} \Big|_{\bar{y}_0 = 0-} + \frac{\partial \bar{p}}{\partial \bar{y}_0} \Big|_{\bar{y}_0 = 0+} \right\} g(0, \bar{z}_0; \bar{y}, \bar{z}) \mathrm{d}\bar{z}_0. \tag{4.18}$$

The physical interpretation of this result is that the total pressure field $\bar{p}$ is given by the incident harmonic wave, $p^{(i)}$, and a perturbation due to the barrier which may be represented in terms of the jump in the horizontal derivative of the pressure integrated over the small height of the barrier. The range of this integral is restricted to the inner region and so we may write the integrand as a Taylor series expansion about $\bar{z}_0 = -h$ (i.e. $\eta_0 = 0$) and exploit the symmetry about this point to obtain

$$g(0, \bar{z}_0; \bar{y}, \bar{z}) = g + \frac{\eta_0^2}{2!} \frac{\partial^2 g}{\partial \eta_0^2} + \frac{\eta_0^4}{4!} \frac{\partial^4 g}{\partial \eta_0^4} + \dots, \tag{4.19}$$

where the Green's functions and its derivatives on the right-hand side of (4.19) are evaluated at $(\bar{y}_0, \bar{z}_0) = (0, -h)$. Upon making the substitutions $\eta_0 = \epsilon Z_0$ and $\mathrm{d}\bar{z}_0 = \epsilon \mathrm{d}Z_0$ in (4.18) we may write

$$\bar{p}(\bar{y}, \bar{z}) = \bar{p}^{(i)}(\bar{y}, \bar{z}) - g(0, -h; \bar{y}, \bar{z}) \int_0^1 \left\{ \frac{\partial P}{\partial Y_0} \Big|_{Y_0 = 0-} + \frac{\partial P}{\partial Y_0} \Big|_{Y_0 = 0+} \right\} \mathrm{d}Z_0$$

$$- \frac{\epsilon^2}{2!} \frac{\partial^2 g}{\partial \bar{z}_0^2}(0, -h; \bar{y}, \bar{z}) \int_0^1 Z_0^2 \left\{ \frac{\partial P}{\partial Y_0} \Big|_{Y_0 = 0-} + \frac{\partial P}{\partial Y_0} \Big|_{Y_0 = 0+} \right\} \mathrm{d}Z_0 + O(\epsilon^4). \tag{4.20}$$

The integrals on the right-hand side of (4.20) are independent of $\bar{y}$ and $\bar{z}$ and are therefore unknown constants, which we may obtain using the matching procedure. Substituting the perturbation expansion (4.9) into the integral terms of (4.20) we find

$$\bar{p}_0(\bar{y}, \bar{z}) = a_{00} \, g(0, -h; \bar{y}, \bar{z}), \tag{4.21}$$

where a_{00} is an as yet unknown coefficient. Similarly, noting that

$$\frac{\partial^2 g}{\partial \bar{y}_0^2} = g - \frac{\partial^2 g}{\partial \bar{z}_0^2} \tag{4.22}$$

we may write the next non-zero term as

$$\overline{p}_2 = a_{20}\, g(0, -h; \overline{y}, \overline{z}) + a_{22}\, \frac{\partial^2 g}{\partial \overline{y}_0^2}(0, -h; \overline{y}, \overline{z}), \tag{4.23}$$

where a_{20} and a_{22} are to be found by matching.

4.2.1. *Near field of the outer solutions*

In order to perform the matching procedure it is necessary to obtain the asymptotic behaviour of $\overline{p}$ as $\overline{r} \to 0$. This may be derived from the integral forms of g, given in (4.15), and its derivatives. Using the identity (see Watson 1966, §6.2)

$$H_0^{(1)}(\overline{r}) = \frac{1}{\pi i} \int_{-\infty}^{\infty} \frac{\exp\{i\alpha\overline{y} - \gamma(\alpha)\eta\}}{\gamma(\alpha)} d\alpha \tag{4.24}$$

we find, after some algebraic manipulation,

$$
\begin{aligned}
g(0, -h; \overline{y}, \overline{z}) &= -\frac{1}{2\pi} \int_{-\infty}^{\infty} \frac{\exp(i\alpha\overline{y})\cosh[\overline{z}\gamma(\alpha)]}{\gamma(\alpha)\sinh[h\gamma(\alpha)]} d\alpha \\
&= \frac{1}{2i} H_0^{(1)}(\overline{r}) - \frac{1}{\pi} \int_{-\infty}^{\infty} \frac{e^{i\alpha\overline{y} - 2h\gamma(\alpha)}\cosh[\eta\gamma(\alpha)]}{\gamma(\alpha)\{1 - e^{-2h\gamma(\alpha)}\}} d\alpha,
\end{aligned} \tag{4.25}
$$

where $\eta = \overline{z} + h$. The integral term on the right-most side of (4.25) converges for all η, $\overline{y}$ and so near $\overline{r} = 0$ we may use a Taylor series expansion to obtain

$$
\begin{aligned}
-\frac{1}{\pi} \int_{-\infty}^{\infty} \frac{e^{i\alpha\overline{y} - 2h\gamma(\alpha)}\cosh[\eta\gamma(\alpha)]}{\gamma(\alpha)\{1 - e^{-2h\gamma(\alpha)}\}} d\alpha &\sim \left(1 - \frac{\eta^2}{2}\right) f_{00} + \left(\frac{\overline{y}^2 - \eta^2}{2}\right) f_{02} \\
&= f_{00}\left(1 - \frac{\overline{r}^2}{4}\right) - \left[\frac{f_{00}}{4} + \frac{f_{02}}{2}\right] \overline{r}^2 \cos 2\theta
\end{aligned} \tag{4.26}
$$

in which the constants f_{00} and f_{02} depend only on the physical parameters of the problem. These are given by

$$f_{00} = -\frac{1}{\pi} \int_{-\infty}^{\infty} \frac{e^{-2h\gamma(\alpha)}d\alpha}{\gamma(\alpha)\{1 - e^{-2h\gamma(\alpha)}\}} \quad \text{and} \quad f_{02} = \frac{1}{\pi} \int_{-\infty}^{\infty} \frac{\alpha^2 e^{-2h\gamma(\alpha)}d\alpha}{\gamma(\alpha)\{1 - e^{-2h\gamma(\alpha)}\}} \tag{4.27}$$

and may be easily and rapidly calculated numerically. Additionally, we may expand the Hankel function $H_0^{(1)}(\overline{r})$ as

$$H_0^{(0)}(\overline{r}) = 1 - \frac{\overline{r}^2}{4} + \frac{2i}{\pi}\left\{\gamma_e + \log\frac{\overline{r}}{2}\right\} + \frac{i\overline{r}^2}{2\pi}\left\{1 - \gamma_e - \log\frac{\overline{r}}{2}\right\} + O(\overline{r}^4), \tag{4.28}$$

where γ_e is Euler's constant ($\simeq 0.577216$). Similarly we may show that

$$
\begin{aligned}
\frac{\partial^2 g}{\partial \overline{y}_0^2}(0, -h; \overline{y}, \overline{z}) &= \frac{1}{2i}\frac{\partial^2}{\partial \overline{y}^2} H_0^{(1)}(\overline{r}) + f_{02} + O(\overline{r}^2) \\
&\sim \frac{\cos 2\theta}{\pi \overline{r}^2} - \frac{\log \overline{r}}{2\pi} + \frac{\cos 2\theta}{4\pi} - \left\{\frac{\gamma_e}{2\pi} + \frac{1}{2\pi}\log\tfrac{1}{2} + \frac{1}{4i} - f_{02}\right\}.
\end{aligned} \tag{4.29}
$$

4.3. *Inner problem*

We must now solve the inner problem for the fluid motion in the vicinity of the barrier in order to determine the constants a_{00}, a_{20}, a_{22} appearing in the outer expansion.

Rewriting (4.2) in terms of the inner variables, P, Y and Z, we find

$$\frac{\partial^2 P}{\partial Y^2} + \frac{\partial^2 P}{\partial Z^2} + \epsilon^2 P = 0, \tag{4.30}$$

and substitution of the perturbation expansion (4.9) gives us, at the first three orders,

$$\frac{\partial^2 P_0}{\partial Y^2} + \frac{\partial^2 P_0}{\partial Z^2} = \frac{\partial^2 P_1}{\partial Y^2} + \frac{\partial^2 P_1}{\partial Z^2} = 0 \quad \text{and} \quad \frac{\partial^2 P_2}{\partial Y^2} + \frac{\partial^2 P_2}{\partial Z^2} + P_0 = 0. \tag{4.31}$$

In this coordinate scaling the free surface has been taken to infinity. Hence we can neglect the effect of the surface and we may also write the impermeability conditions in terms of $P^{(i)}$, the pressure field associated with the incident Rossby wave expressed in the inner coordinates. Thus, the bottom condition gives us $P_Z = 0$ on $Z = 0$ and the imposition of no normal flow through the barrier requires that on $Y = 0$, $0 < Z < 1$,

$$P = -P^{(i)} = \cos\left[\pi(1 - \mu)Z\right] = 1 - \frac{\pi^2 f_0^2 \epsilon^2 Z^2}{2 N_0^2 H^2 K^2} + O(\epsilon^4). \tag{4.32}$$

The problem then reduces to solving the Laplace equation (for P_0 and P_1) or the Poisson equation (P_2 and higher) subject to these boundary conditions.

4.3.1. *Zeroth- and second-order inner solutions*

The reduced equations of motion and the boundary conditions given above are even in both Y and Z and therefore we may restrict our solutions to those similarly even in Y and Z. It is clear, therefore, that P_1 (and, in general, P_{2n+1}) must be identically zero. It may be shown (see Morse & Feshbach 1953, §10.1) that the homogeneous boundary value problem has eigensolutions most easily expressed in the form

$$F_n(\xi, \phi) = \begin{cases} \xi, & n = 0, \\ \sinh n\xi \cos\left[n(\phi - \tfrac{1}{2}\pi)\right], & n = 1, 2, 3\ldots, \end{cases} \tag{4.33}$$

where ξ and ϕ are elliptic coordinates defined by

$$\xi + i\phi = \cosh^{-1}(Z + iY). \tag{4.34}$$

In order to perform the matching procedure we shall also define the polar coordinates (4.6) R and θ by $R \exp i\theta = Z + iY$. It may be shown that as $R \to \infty$ these coordinate systems are related by

$$\xi = \log 2R - \frac{\cos 2\theta}{4R^2} + O(R^{-4}) \quad \text{and} \quad \phi = \theta + \frac{\sin 2\theta}{4R^2} + O(R^{-4}). \tag{4.35}$$

The eigenfunctions of the inner problem, therefore, are such that F_n grows no faster than R^n, or $\log R$ when $n = 0$. We may now write down an expression for the leading-order solution in terms of a (constant) particular solution which satisfies the appropriate boundary conditions (4.32) and the inner eigensolutions (4.33). From the form of the outer solutions given in (4.21) and (4.23), and in anticipation of the application of the matching procedure, it may be seen that in general P_m contains eigenfunctions only up to F_m. Thus, we have

$$P_0 = 1 + A_{00} F_0(\xi, \phi) \tag{4.36}$$

In order to find the second-order inner solution it may be seen from (4.31) that P_2 satisfies the biharmonic equation, $\nabla^4 P_2 = 0$. We may therefore write the general

solution in the form

$$P_2(Y,Z) = \mathrm{Re}\left\{[Z - \mathrm{i}Y]G_1(Z + \mathrm{i}Y) + [Z + \mathrm{i}Y]G_2(Z - \mathrm{i}Y)\right\}, \qquad (4.37)$$

where G_1 and G_2 are arbitrary analytic functions. We may substitute (4.37) into the Poisson equation, $\nabla^2 P_2 = -P_0$, and directly integrate to obtain a particular solution. Omitting details, it may be shown that the most general solution of the Poisson equation which satisfies the correct boundary condition on the barrier and the radiation condition given above is

$$P_2 = -\frac{R^2}{4} + \left\{\frac{1}{4} + \frac{\pi^2 f_0^2}{2N_0^2 H^2 K^2}\right\} R^2 \cos 2\theta + A_{20} F_0(\xi, \phi) + A_{22} F_2(\xi, \phi)$$

$$-A_{00}\left\{\frac{R^2}{4}\mathrm{Re}\left[\cosh^{-1}(R\mathrm{e}^{\mathrm{i}\theta})\right] - \frac{1}{4}\mathrm{Re}\left[R\mathrm{e}^{-\mathrm{i}\theta}\{R^2\mathrm{e}^{2\mathrm{i}\theta} - 1\}^{1/2}\right]\right\}. \qquad (4.38)$$

It is easy to show that $-P_2$ is equal to the coefficient of the ϵ^2 term in (4.32) on the barrier, because F_0 and F_2 vanish there by construction, and the last term in parentheses is also zero by inspection. We are now in a position to apply the matching procedure in order to determine the unknown coefficients A_{ij} and a_{ij}.

4.4. *Matching procedure*

In order to determine the six unknown constants a_{00}, a_{20}, a_{22}, A_{00}, A_{20}, and A_{22} defined above we shall use the matching procedure given in Van Dyke (1964). It is worth recalling here that we treat any $\log \epsilon$ terms as constants during matching, which as a consequence are absorbed into these six coefficients. Denote the asymptotic forms of the inner and outer pressure fields by

$$P^{(a)} = \sum_{n=0}^{a} \epsilon^n P_n \quad \text{and} \quad \overline{p}^{(a)} = \sum_{n=0}^{a} \epsilon^n \overline{p}_n \qquad (4.39)$$

respectively. Now we may write the inner pressure $P^{(a)}$ in terms of the outer variables $\overline{y} = \epsilon Y$, $\eta = \epsilon Z$, and further expand in powers of ϵ. We truncate the expression at order ϵ^a and denote this by $P^{(a,b)}$. Similarly, we may form $\overline{p}^{(b,a)}$ by rewriting $\overline{p}^{(b)}$ in terms of the inner variables and truncating at order ϵ^a. The matching principle then states that

$$P^{(a,b)} \equiv \overline{p}^{(b,a)}. \qquad (4.40)$$

Performing the expansion and truncation on the lowest-order solutions we find

$$P^{(0,0)} = 1 + A_{00}\log\frac{2}{\epsilon} + A_{00}\log\overline{r} \qquad (4.41)$$

and

$$\overline{p}^{(0,0)} = a_{00}\left\{\frac{1}{2\mathrm{i}} + \frac{\gamma_e}{\pi} + \frac{1}{\pi}\log\tfrac{1}{2} + f_{00}\right\} + \frac{a_{00}}{\pi}\log\overline{r}, \qquad (4.42)$$

and thus

$$a_{00} = \pi A_{00} = \left\{\frac{1}{2\mathrm{i}} + \frac{\gamma_e}{\pi} + \frac{1}{\pi}\log\frac{\epsilon}{4} + f_{00}\right\}^{-1}. \qquad (4.43)$$

At the second order we have

$$\overline{p}^{(0,2)} = \overline{p}^{(0,0)} + a_{00}\overline{r}^2\left[\frac{1}{4\pi}\{1 - \gamma_e - \log\tfrac{1}{2}\} - \frac{1}{8\mathrm{i}} - \frac{f_{00}}{4}\right]$$

$$-\frac{a_{00}}{4\pi}\overline{r}^2\log\overline{r} - \frac{a_{00}}{4}\overline{r}^2\cos 2\theta\left[f_{00} + 2f_{02}\right] \qquad (4.44)$$

and

$$P^{(2,0)} = P^{(0,0)} + \frac{\bar{r}^2}{4}\left[A_{00}\left\{1 + \log\frac{\epsilon}{2}\right\} - 1\right] - \frac{A_{00}}{4}\bar{r}^2\log\bar{r}$$

$$+\bar{r}^2\cos 2\theta\left[2A_{22} + \tfrac{1}{4} + \frac{\pi^2 f_0^2}{2N_0^2 H^2 K^2}\right]. \quad (4.45)$$

Comparison of the $\bar{r}^2$ and $\bar{r}^2\log\bar{r}$ terms gives the same form for a_{00} and A_{00} as (4.43) and acts as a consistency check for the matching procedure. Comparison of the $\bar{r}^2\cos 2\theta$ terms enables us to show that A_{22} is given by

$$A_{22} = -\frac{1}{8} - \frac{\pi^2 f_0^2}{4N_0^2 K^2 H^2} - \frac{a_{00}}{8}\left[f_{00} + 2f_{02}\right]. \quad (4.46)$$

Similarly, it may be shown that

$$\bar{p}^{(2,0)} = \bar{p}^{(0,0)} + \frac{a_{22}}{\pi}\frac{\cos 2\Theta}{R^2} \quad \text{and} \quad P^{(0,2)} = P^{(0,0)} - A_{00}\frac{\cos 2\theta}{4R^2} \quad (4.47)$$

and thus $a_{22} = -\pi A_{00}/4 = -a_{00}/4$. Finally, performing the highest-order matching we obtain

$$\bar{p}^{(2,2)} = \bar{p}^{(2,0)} + \epsilon^2\frac{a_{22}}{4\pi}\cos 2\theta + \frac{\epsilon^2}{\pi}\{a_{20} - a_{22}\}\log\bar{r}$$

$$+\epsilon^2 a_{20}\left\{\frac{1}{2i} + \frac{\gamma_e}{\pi} + \tfrac{1}{2}\log\tfrac{1}{2} + f_{00}\right\} - \epsilon^2 a_{22}\left\{\frac{1}{4i} + \frac{\gamma_e}{2\pi} + \frac{1}{2\pi}\log\tfrac{1}{2} - f_{02}\right\} \quad (4.48)$$

and

$$P^{(2,2)} = P^{(0,2)} - \epsilon^2\left\{A_{22} + A_{20}\log\frac{2}{\epsilon}\right\} - \epsilon^2\frac{A_{00}}{16}\cos 2\theta + \epsilon^2 A_{20}\log\bar{r}. \quad (4.49)$$

Comparison of the $\epsilon^2\cos 2\theta$ terms serves as a consistency check for the relationship between a_{22} and A_{00}. Comparison of the remaining terms enables us to form a pair of simultaneous equations expressing the unknowns a_{20} and A_{20}, namely

$$a_{20}\left\{\frac{1}{2i} + \frac{\gamma_e}{\pi} + \frac{1}{\pi}\log\tfrac{1}{2} + f_{00}\right\} + A_{20}\log\frac{2}{\epsilon} = a_{22}\left\{\frac{1}{4i} + \frac{\gamma_e}{2\pi} + \frac{1}{2\pi}\log\tfrac{1}{2} - f_{02}\right\} - A_{22},$$

$$(4.50)$$

$$a_{20} - \pi A_{20} = a_{22}, \quad (4.51)$$

which may be readily solved.

4.5. *Recovery of the normal-mode solution*

Having determined the unknown matching coefficients a_{00}, a_{20} and a_{22} we may construct the approximate outer solution in terms of reflection and transmission coefficients for the normal mode. Deforming the integration contour in (4.15) into the upper or lower half-plane as appropriate shows that, in the far field,

$$g(0, -h; \bar{y}, \bar{z}) = -i\sum_{n=0}^{\lfloor h/\pi\rfloor}(-1)^n\frac{\epsilon_n}{2h\alpha_n}\exp(i\alpha_n|\bar{y}|)\cos\frac{n\pi\bar{z}}{h}, \quad (4.52)$$

where $\alpha_n^2 = 1 - n^2\pi^2/h^2$, ϵ_n is as in (2.6) and $\lfloor x\rfloor$ denotes the greatest integer less than x. The terms for which α_n is imaginary correspond to evanescent modes and have
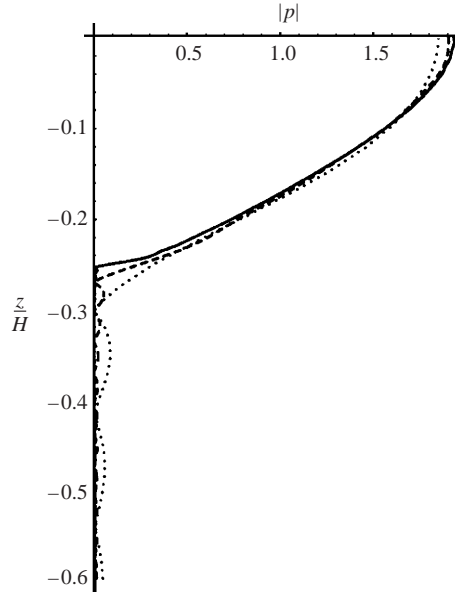
FIGURE 4. Pressure field above a barrier of height $0.75H$ for parameter values specified in §5.1. Dotted, dashed and solid lines refer to truncation numbers 8, 30 and 120 respectively.

been neglected. Similarly, we have

$$\frac{\partial^2 g}{\partial \bar{y}_0^2}(0, -h; \bar{y}, \bar{z}) = i \sum_{n=0}^{\lfloor h/\pi \rfloor} (-1)^n \frac{\alpha_n \epsilon_n}{2h} \exp(i\alpha_n |\bar{y}|) \cos\frac{n\pi\bar{z}}{h}. \tag{4.53}$$

The z dependence of these terms is identical to the vertical normal-mode structure derived in §3 and so using (4.21) and (4.23) we may numerically determine the coefficients of the propagating modes.

5. Numerical results

5.1. *Algebraic method*

Having found the unknown coefficients $\alpha_1, \dots, \alpha_m$ we may reconstruct the vertical variation of the total pressure field above the barrier. Unless otherwise stated we shall use the parameters $H = 4000\,\text{m}$, $N = 0.02\,\text{s}^{-1}$, $\theta = 45°$, $f_0 = 1.03 \times 10^{-4}\,\text{s}^{-1}$ and $\beta = 1.62 \times 10^{-11}\,\text{s}^{-1}\,\text{m}^{-1}$, which corresponds to the origin of the β-plane at 45°N, and $\omega = 4.04 \times 10^{-7}\,\text{s}^{-1}$, which represents a period of 180 days. For these parameters there are four propagating modes. The truncation number is set at $M = 300$ unless specifically quoted in the text. Figure 4 shows the total pressure field structure above a barrier of height $0.75H$. The dotted, dashed and solid lines in figures 4 and 5 denote the solution generated by truncation at 8, 30 and 120 terms respectively. We see a good degree of convergence to a solution with zero pressure on the barrier (as required by quasi-geostrophy) as the number of terms increases. At the barrier tip, the pressure increases rapidly and this is in accordance with the singularity in the analytic solution which may be found by considering the fluid flow near this point.

Figure 5 shows the total pressure field structure above a barrier of height $0.25H$. As with the previous figure, this also exhibits good convergence as the size of the truncated system increases, as well as the same qualitative behaviour at the barrier
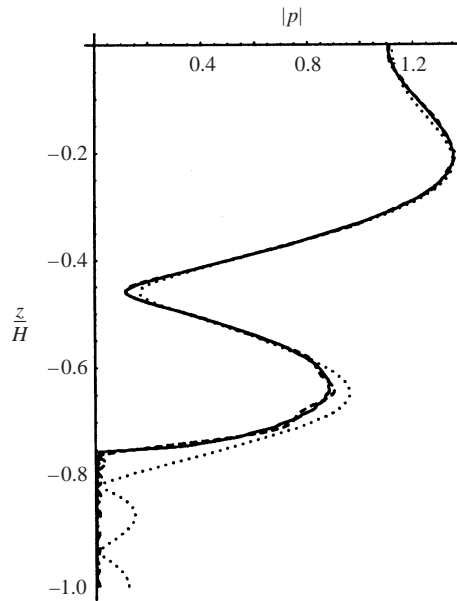
FIGURE 5. Pressure field above a barrier of height $0.25H$ for parameter values specified in §5.1. Dotted, dashed and solid lines refer to truncation numbers 8, 30 and 120 respectively.

tip. However, the pressure field is no longer monotonic and there is a local minimum located at a height comparable to the nodal point in the incident pressure field.

We may also contrast the reflection coefficients for the modes other than the incident mode. Figure 6 shows the reflection coefficients a_n for the propagating modes when $\theta = 30°$ and $60°$ and the ridge height varies from H ($\mu = 0$) to 0 ($\mu = 1$). Note that the number of propagating modes varies with barrier angle (due to k_n changing with θ, see (2.8)), and for the parameters chosen there are, as shown, three modes cut-on at $\theta = 30°$ and five modes at $\theta = 60°$. By way of comparison, figures 7(a) and 7(b) illustrate the coefficients when the incident waves are the second and third baroclinic modes respectively. In these cases the curves tend to be more oscillatory than for the mode 1 forcing, which is due to the more oscillatory vertical pressure variation of the higher modes. For example, the magnitude of the reflected barotropic wave has n maxima for an incident baroclinic wave of mode n. Due to anisotropy of the governing equation (2.2), there does not appear to be a simple reciprocity relation between modes, such as would be available in classical water wave or acoustic models. Despite this, figures 6 and 7 demonstrate behaviour near to reciprocity between the modes: figure 6(b) shows the reflection coefficient curves of $|a_2|$ and $|a_3|$ for an incident wave of mode 1, and these are very close to the $|a_1|$ curves in figure 7 due to incident mode 2 and 3 waves respectively. Similarly, figure 7(a) shows that the plot of $|a_3|$ for an incident second-mode baroclinic wave is of similar form to the mode 2 reflection coefficient (scattered from an incident mode 3 wave) given in figure 7(b).

It is clear from figures 6 and 7 that it is quite possible for modes other than the incident wave to be the most energetic scattered component. Indeed, it may be noted that, for moderate values of μ, an incident wave will tend to scatter its energy quite efficiently into its neighbouring modes, e.g. in figure 7(b) the second and fourth baroclinic modes are of comparable amplitude to the reflected third mode. More generally, figure 8 shows the reflection coefficient of the incident mode $|a_1|$ for a complete range of barrier orientations, θ, and non-dimensional gap heights, μ. The
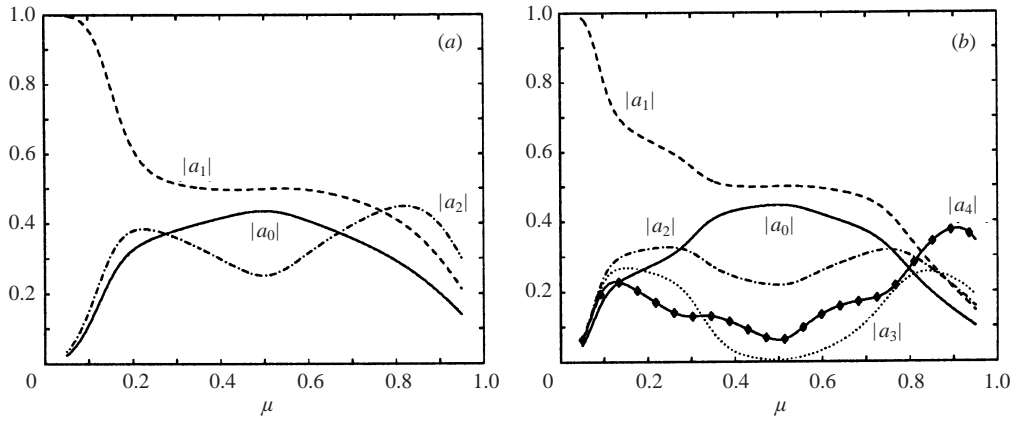
FIGURE 6. Reflection coefficients for barotropic and propagating baroclinic modes. The incident wave is the first baroclinic mode and $\theta = 30°$ and $60°$ in (a) and (b), respectively.
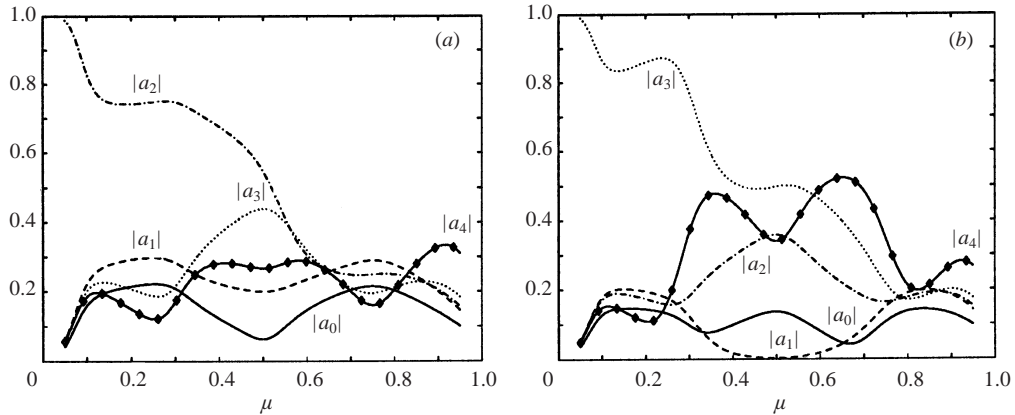

FIGURE 7. Reflection coefficients for barotropic and propagating baroclinic modes with barrier angle $\theta = 60°$. The incident waves are the second and third baroclinic modes in (a) and (b), respectively.

rapid variation visible near $\theta = 20°$ and, to a lesser extent, $\theta = 35°$ and $\theta = 55°$ corresponds to the angles at which the highest propagating mode is cut-on i.e. its wavenumber becomes real.

In order to demonstrate the efficacy of the algebraic method employed herein, figure 9 is presented for the typical parameter values stated at the beginning of this section with $\mu = 0.75$, and reveals the convergence of the reflection coefficient $|a_1|$ with increasing truncation number. The data are shown in the manner of figure 2 of McIver (1985), which discussed a related problem in linear water wave theory and offered an alternative algebraic method of solution. McIver's approach required a truncation number of order 400 and a further linear interpolation to find the zeros of reflection to three significant figures of accuracy. In contrast, the method in the present work produces reflection coefficients with an additional significant figure of accuracy at the same truncation number, and therefore removes the need for an interpolation step.

5.2. *Asymptotic method and comparison*

Figures 10 and 11 show the comparison between the predictions from the asymptotic and algebraic methods, when $1 - \mu \ll 1$. Illustrated are the propagating-mode reflec-
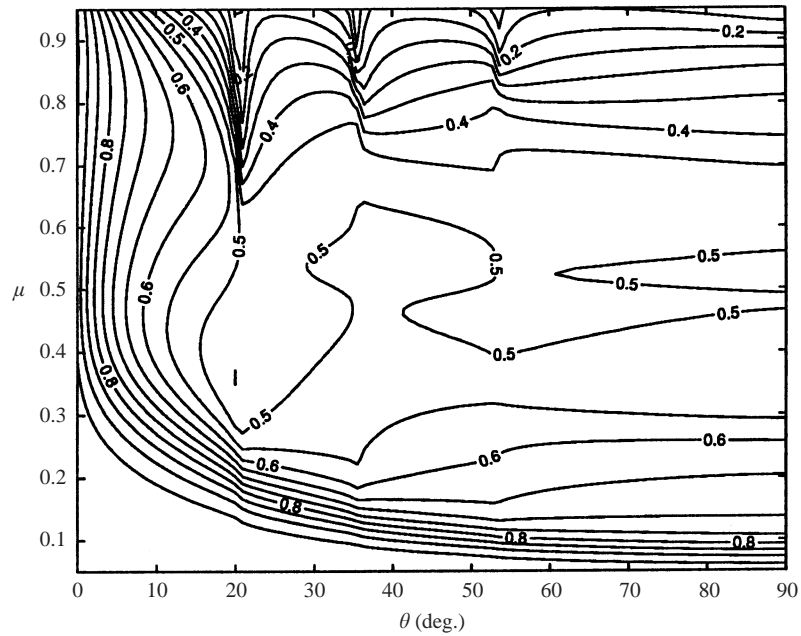
FIGURE 8. Contour plot of reflection coefficient $|a_1|$ over all ridge heights and orientations.
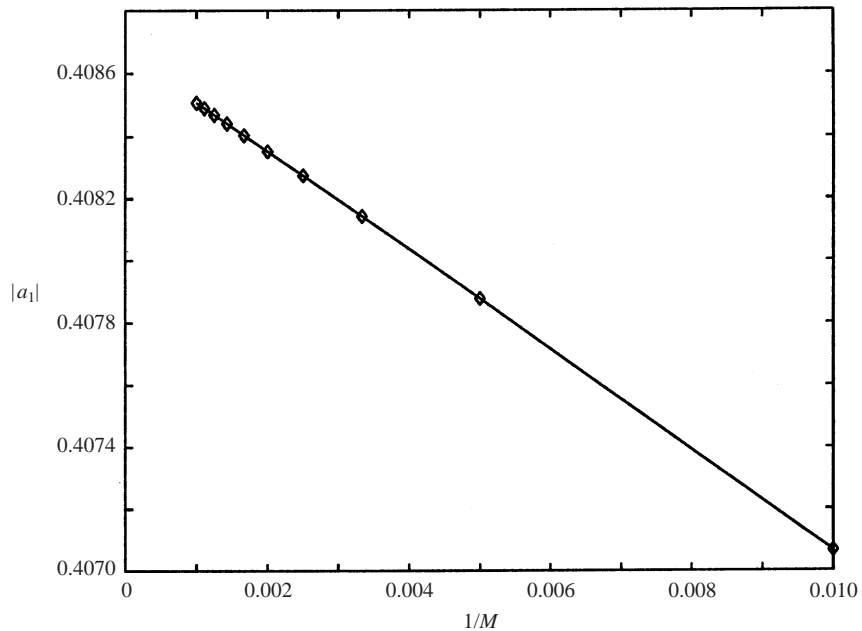

FIGURE 9. Reflection coefficient $|a_1|$ against the reciprocal of the truncation number, M.
Plotted points are for $M = 100, 200, \ldots, 1000$.

tion coefficients for, respectively, $\theta = 30°$ and $60°$ over μ values close to unity; solid lines refer to the solution of the algebraic system and dashed lines are the asymptotic results. The generation of the points by the algebraic technique requires considerably more computation time than for moderate values of μ, whereas the asymptotic results
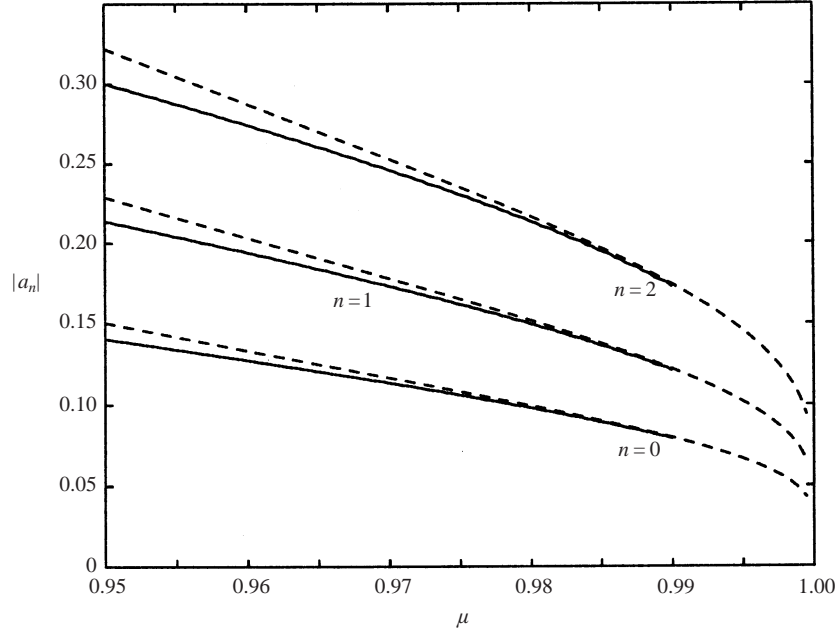
FIGURE 10. Reflection coefficients of propagating modes with ridge angle $\theta = 30°$. The dashed and solid lines represent the asymptotic and algebraic solutions, respectively.

may be numerically evaluated very rapidly. Furthermore, the agreement between the two methods over the range for which they are both accurate implies that the solution to which the algebraic scheme converges is correct. It can also be seen that when the barrier is small the incident wave is scattered into several modes, the highest of which is preferentially reflected. Physically, this corresponds to the fact that ridges of small height channel the incident energy into waves with vertical scale comparable to the ridge height. From the symmetry, this effect also occurs in the component of the transmitted wave field corresponding to the perturbation induced by the ridge. However, for small barriers the transmission coefficient of the incident mode is $O(1)$, and thus the incident wave will also be the dominant transmitted mode.

Considering the horizontal velocity and vertical displacement fields it may be shown (LeBlond & Mysak 1978, § 18) that the mean kinetic and potential energy densities for a long Rossby wave of mode n, that is

$$p = A_n \exp\{i\mathbf{k} \cdot \mathbf{x} + i\omega t\}\Gamma_n(z), \tag{5.1}$$

are given by

$$\langle KE \rangle = \frac{|A_n^2||\mathbf{k}|^2}{4f_0^2} \int_{-H}^{0} \frac{\Gamma_n^2}{\rho_0}\,\mathrm{d}z \quad \text{and} \quad \langle PE \rangle = \frac{|A_n^2|}{gh_n} \int_{-H}^{0} \frac{\Gamma_n^2}{\rho_0}\,\mathrm{d}z, \tag{5.2}$$

respectively. Figure 12 shows the most energetic transmitted mode number for a range of values in θ, μ parameter space; for example, when $\mu = 0.5$, $\theta = 45°$ the $n = 1$ mode has the highest total energy, $\langle KE \rangle + \langle PE \rangle$. As expected, it may be shown that when the barrier is small the incident wave, $n = 1$, is the most energetic. However, for values of $1 - \mu$ of the order of 0.1 it is possible for other transmitted modes to be more energetic than the transmitted $n = 1$ mode. This is particularly true when the ridge is orientated nearly meridionally, such as is the case with the mid-Atlantic
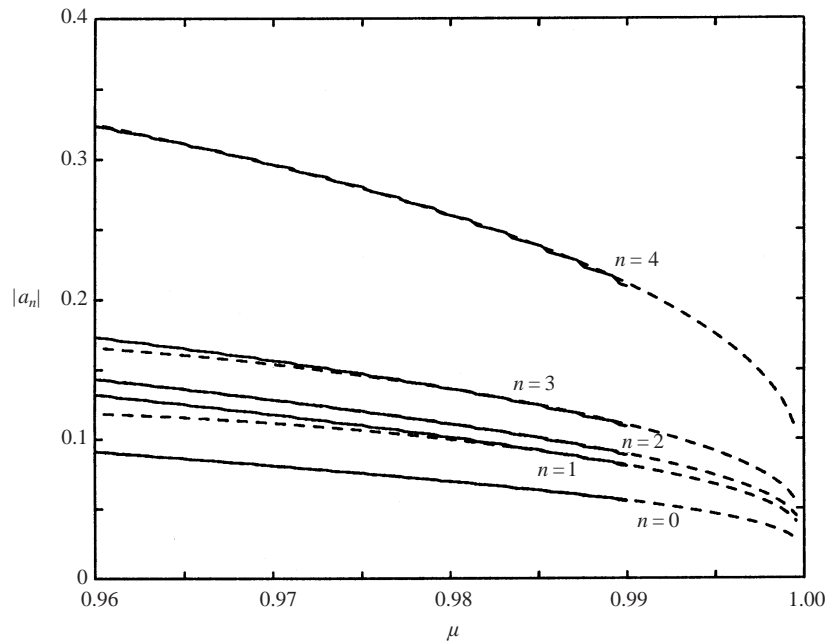
FIGURE 11. Reflection coefficients of propagating modes with $\theta = 60°$. The dashed and solid lines represent the asymptotic and algebraic solutions, respectively.
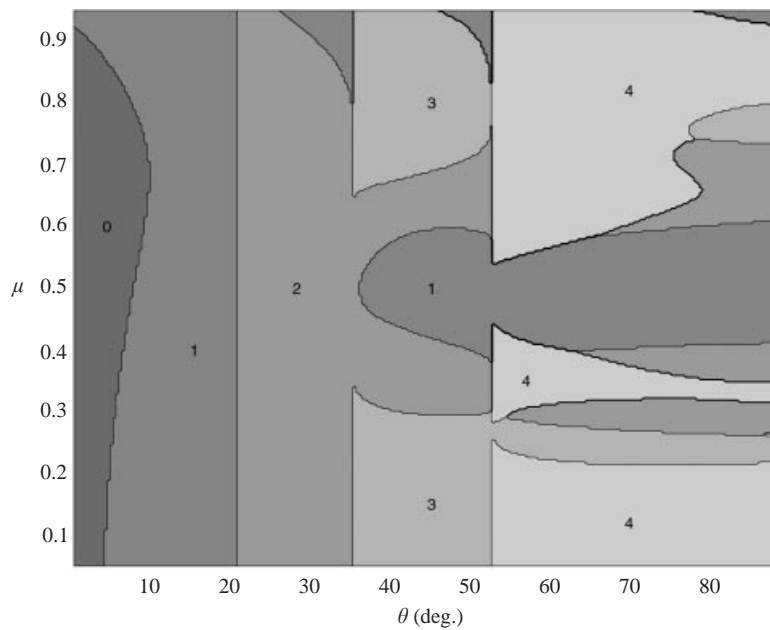

FIGURE 12. Most energetic transmitted mode number for each region in parameter space μ, θ.

ridge, and the 90°E ridge in the Indian Ocean. Further, it may be noted that when the tip of the barrier is near to a nodal point in the vertical pressure variation (i.e. $\mu = 1/2$ for mode 1 and $\mu = 1/3$ or $2/3$ for mode 2) then there is a tendency for these modes to be scattered more energetically than in general. Finally, figure 13 shows the difference in phase (in radians) between this most energetic transmitted mode and
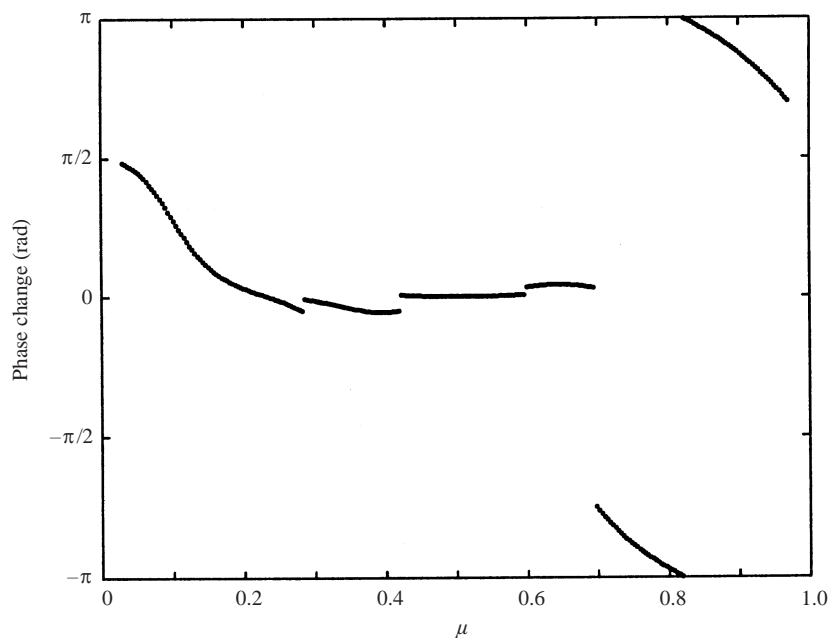
FIGURE 13. Phase change between incident and most energetic transmitted modes, $\theta = 45°$.

the incident wave. It can be seen that for values of $1 - \mu$ of the order 0.1 to 0.3, when mode 3 is the most energetic, this phase change is appreciable.

6. Conclusions

The addition of continuous stratification in the present model improves the physical relevance of this work compared to previous studies. In particular, results in § 5 reveal the extent to which a submerged ocean ridge can scatter an incident westward-propagating long baroclinic Rossby wave into the other modes. However, continuous stratification does add somewhat to the mathematical difficulty of the scattering problem. The infinite modal structure requires the solution of an infinite system, and we have devised a scheme for the solution which is successful for a wide range of parameter values, regardless of the particular choice of density variation. The approach is, however, dependent on obtaining accurate numerical solutions to the eigenvalue problem (2.5). In contrast, application of the asymptotic method, as applied herein, is reliant on the choice of constant density gradient and application to a different, more realistic, stratification would in general require a reciprocity relation to serve the role of Green's theorem in the derivation in § 4.2. The coincidence between the algebraic and asymptotic solutions in figures 10 and 11, however, serves as a check that in the case of linear density variation our algebraic approach is indeed converging to the correct solution.

Although figure 6 shows that the zeroth mode can be excited with a fairly large coefficient, the barotropic nature of the vertical structure means that the wave has no mean potential energy. It transpires that the region in parameter space in which this mode is the most energetic is fairly small, corresponding to near oblique incidence when only the $n = 0$ and $n = 1$ cut-on modes are present. In parameter regimes in which higher-order (and more energetic) modes can propagate, these modes can be generated by relatively small topography, on the scale of $1 - \mu = 0.05$, which

corresponds to ocean ridges of the order of 200 m. It can be expected that the greater energy in the excited (non-incident) mode would lead to its signature being more prominent on altimetry data. Furthermore, such mode conversion will in general result in a phase change in the transmitted wave (see figure 13) and it is hypothesized that the excitation of non-incident modes would explain the discontinuity in phase undergone during interactions with topography, as observed recently in Along Track Scanning Radiometer data by Hill *et al.* (2000, §7.3). Figure 10(*a*) of the latter paper reveals phase discontinuities in the measured field as Rossby waves propagate across the Mid-Atlantic Ridge at 20°W, and in the Indian Ocean at the 90°E and Central Indian Ridges. These features may be especially prominent in Hill *et al.*'s (2000) data for two reasons. First, their data analysis of the Hovmüller plots preferentially selects the slower (higher) modes and, second, these higher modes (and especially mode 3) have stronger thermal signatures than the first mode. As can be seen in figure 13, our theoretical model suggests a very significant phase shift across the barrier between an incident mode 1 wave and a transmitted mode 3 wave. There is also some direct evidence of Rossby wave mode conversion across ocean ridges in Hill *et al.* (2000), again visible in figure 10(*a*) of their article, via the change in angle of the wavecrests across a ridge. Comparable data are also available via TOPEX/POSEIDON, but in both cases further activity is needed in order to establish a quantitative link with the present work.

In terms of further research, two clear avenues present themselves. First, in order to model more realistically actual ocean processes, we should consider a stratification that better represents some of the major features of the thermocline. Garrett & Munk (1972) derived piecewise-exponential best fit profiles from experimental data and this also leads to an eigenvalue problem which may be solved analytically, albeit with a little more difficulty than the constant-N_0 case used above. Alternatively, Emery, Lee & Magaard (1984) produced profiles of the Brunt–Väisälä frequency for the Atlantic and Pacific Oceans from hydrographic data. Using such a profile it should be possible to obtain the vertical modal structure accurately by standard numerical methods. Secondly, our model topography may be made more complex. For example, we believe that a periodic barrier containing gaps is a better model of real topography and that the scattering by such a ridge may be found using a variation on the algebraic method employed above. This is currently under investigation by the authors, as is the effect of mean flow on the scattering by a submerged ridge.

REFERENCES

ABRAHAMS, I. D. 1987 Scattering of sound by two parallel semi-infinite screens. *Wave Motion* **9**, 289–300.

ABRAHAMS, I. D. & WICKHAM, G. R. 1992 Scattering of elastic waves by an arbitrary small imperfection in the surface of a half-space. *J. Mech. Phys. Solids* **40**(8), 1683–1706.

ANDERSON, D. L. T. & KILLWORTH, P. D. 1977 Spin-up of a stratified ocean with topography. *Deep-Sea Res.* **24**, 709–732.

CHELTON, D. B. & SCHLAX, M. G. 1996 Global observations of oceanic Rossby waves. *Science* **272**, 234–238.

CRIGHTON, D. G., DOWLING, A. P., FFOWCS WILLIAMS, J. E., HECKL, M. & LEPPINGTON, F. G. 1992 *Modern Methods in Analytical Acoustics. Lecture Notes.* Springer.

CUSHMAN-ROISIN, B. 1994 *Introduction to Geophysical Fluid Dynamics.* Prentice Hall.

DEWAR, W. K. 1998 On "too fast" baroclinic planetary waves in the general circulation. *J. Phys. Oceanogr.* **28**, 1739–1758.

DEWAR, W. K. & MORRIS, M. Y. 2000 On the propagation of baroclinic waves in the general circulation. *J. Phys. Oceanogr.* **30**, 2637–2649.

EMERY, W. J., LEE, W. G. & MAGAARD, L. 1984 Geographical and seasonal distributions of Brunt–Väisälä frequency and Rossby radii in the North Pacific and North Atlantic. *J. Phys. Oceanogr.* **14**, 294–317.

EMERY, W. J. & MAGAARD, L. 1976 Baroclinic Rossby waves as inferred from temperature fluctuations in the eastern Pacific. *J. Mar. Res.* **34**, 365–385.

GARRETT, C. J. R. & MUNK, W. H. 1972 Space-time scales of internal waves. *Geophys. Fluid Dyn.* **3**, 225–264.

HILL, K. L., ROBINSON, I. S. & CIPOLLINI, P. 2000 Propagation characteristics of extratropical planetary waves observed in the ATSR global sea surface temperature record. *J. Geophys. Res.* **105**(C9), 21927–21946.

HUGHES, C. W. 1995 Rossby waves in the Southern Ocean: a comparison of TOPEX/POSEIDON altimetry with model predictions. *J. Geophys. Res.* **100**(C8), 15933–15950.

HUGHES, C. W., JONES, M. S. & CARNOCHAN, S. 1998 Use of transient features to identify eastward currents in the Southern Ocean. *J. Geophys. Res.* **103**(C2), 2929–2943.

HUTHNANCE, J. M. 1981 A note on baroclinic Rossby-wave reflection at sea-floor scarps. *Deep-Sea Res.* A **28**, 83–91.

JOHNSON, E. R. 1989 The low-frequency scattering of Kelvin waves by stepped topography. *J. Fluid Mech.* **215**, 23–44.

JOHNSON, E. R. 1991 The scattering at low-frequencies of coastally trapped waves. *J. Phys. Oceanogr.* **21**, 913–932.

KILLWORTH, P. D. & BLUNDELL, J. R. 1999 The effect of bottom topography on long extratropical planetary waves. *J. Phys. Oceanogr.* **29**, 2689–2710.

KILLWORTH, P. D., CHELTON, D. B. & DE SZOEKE, R. A. 1997 The speed of observed and theoretical long extratropical planetary waves. *J. Phys. Oceanogr.* **27**, 1946–1966.

LEBLOND, P. H. & MYSAK, L. A. 1978 *Waves in the Ocean.* Elsevier.

MCIVER, P. 1985 Scattering of water waves by two surface piercing vertical barriers. *IMA J. Appl. Maths* **35**, 339–355.

MORSE, P. M. & FESHBACH, H. 1953 *Methods of Theoretical Physics.* McGraw-Hill.

MURPHY, D. G. & WILLMOTT, A. J. 1991 Rossby-wave scattering by a meridional barrier in an infinitely long zonal channel. *J. Phys. Oceanogr.* **21**, 621–634.

MYSAK, L. A. & LEBLOND, P. H. 1972 The scattering of Rossby waves by a semi-infinite barrier. *J. Phys. Oceanogr.* **2**, 108–114.

PEDLOSKY, J. 1979 *Geophysical Fluid Dynamics.* Springer.

PEDLOSKY, J. 2000a The transmission and transformation of baroclinic Rossby waves by topography. *J. Phys. Oceanogr.* **30**, 3077–3101.

PEDLOSKY, J. 2000b The transmission of Rossby waves through basin barriers. *J. Phys. Oceanogr.* **30**, 495–511.

PEDLOSKY, J. 2001 The transparency of ocean barriers of Rossby waves: The Rossby slit problem. *J. Phys. Oceanogr.* **31**, 336–352.

PEDLOSKY, J. & SPALL, M. 1999 Rossby normal modes in basins with barriers. *J. Phys. Oceanogr.* **29**, 2332–2349.

PORTER, R. & EVANS, D. V. 1995 Complimentary approximations to wave scattering by vertical barriers. *J. Fluid Mech.* **294**, 155–180.

QIU, B., MIAO, W. F. & MULLER, P. 1997 Propagation and decay of forced and free baroclinic Rossby waves in off equatorial oceans. *J. Phys. Oceanogr.* **27**, 2405–2417.

RHINES, P. B. 1969 Slow oscillations in an ocean of varying depth. Part 1. Abrupt topography. *J. Fluid Mech.* **37**, 161–189.

SCHMIDT, G. A. & JOHNSON, E. R. 1997 The scattering of stratified Rossby waves by seafloor ridges *Geophys. Astrophys. Fluid Dyn.* **84**, 29–52.

VAN DYKE, M. D. 1964 *Perturbation Methods in Fluid Mechanics.* Parabolic.

WANG, L. P. & KOBLINSKY, C. J. 1994 Influence of mid-ocean ridges on Rossby waves. *J. Geophys. Res.* **99**(C12), 26143–25153.

WATSON, G. N. 1966 *A Treatise on the Theory of Bessel Functions*, 2nd Edn. Cambridge University Press.